Company, Southern California Edison Company, The Standard Oil Company, and University of Rochester. Such support does not imply endorsement of the content by any of the above parties.

REFERENCES

1. S. Skupsky and K. Lee, *J. Appl. Phys.* **54**, 3662 (1983).

2. S. R. Gunn, *J. Phys. E* **6**, 105 (1973).

2.B Holographic Wave-Front Measurement of the GDL Frequency-Converted Laser Beam

One of the current objectives of the uniformity activity at the LLE is to determine the factors which control the quasi-far-field intensity distribution of the individual frequency-converted laser beams and to determine the extent to which these factors can be manipulated to optimize overall irradiation uniformity on a target.[1] Measurement techniques, which generate near-field intensity and phase distributions, as well as quasi-far-field intensity distributions of individual laser beams, are essential in fulfilling these objectives. Holographic wavefront measurement is capable of recording all of the information necessary for the complete recovery of the original complex amplitude distribution. Holographically generated near-field intensity and phase profiles, together with a two-dimensional (2-D) beam propagation code, constitute a predictive tool for the calculation of the quasi-far-field intensity distribution at any given target plane.[2] Furthermore, computer-based amplitude and phase modulation studies could be performed with the use of this predictive tool, and experimental corroboration would be possible with a continuum of cw, holographically reconstructed, quasi-far-field profiles of the pulsed laser beam.

Conventional Wave-Front Measurement

Wave-front-measurement techniques, previously used at 1054 nm, were redesigned for use on the GDL frequency-tripled laser beam as shown in Fig. 18.3. GDL is characterized by the following parameters:

Wavelength	351 nm
Energy	0-70 J
Pulse Width	850 ps (FWHM)
Diameter	125 mm
Polarization	linear, vertical

The first path transports the beam through a focusing lens and into an equivalent-target-plane (ETP) camera. The focusing beam is injected into a 1° wedged beam splitter (reflectivity = 70% both surfaces), thus producing both a transmitted and a reflected one-dimensional (1-D) array in exposure. The reflected array contains several images which differ in intensity by one-half. The intensity of the first image is larger than the others in order to check for the high-intensity photographic errors characteristic of a limited dynamic

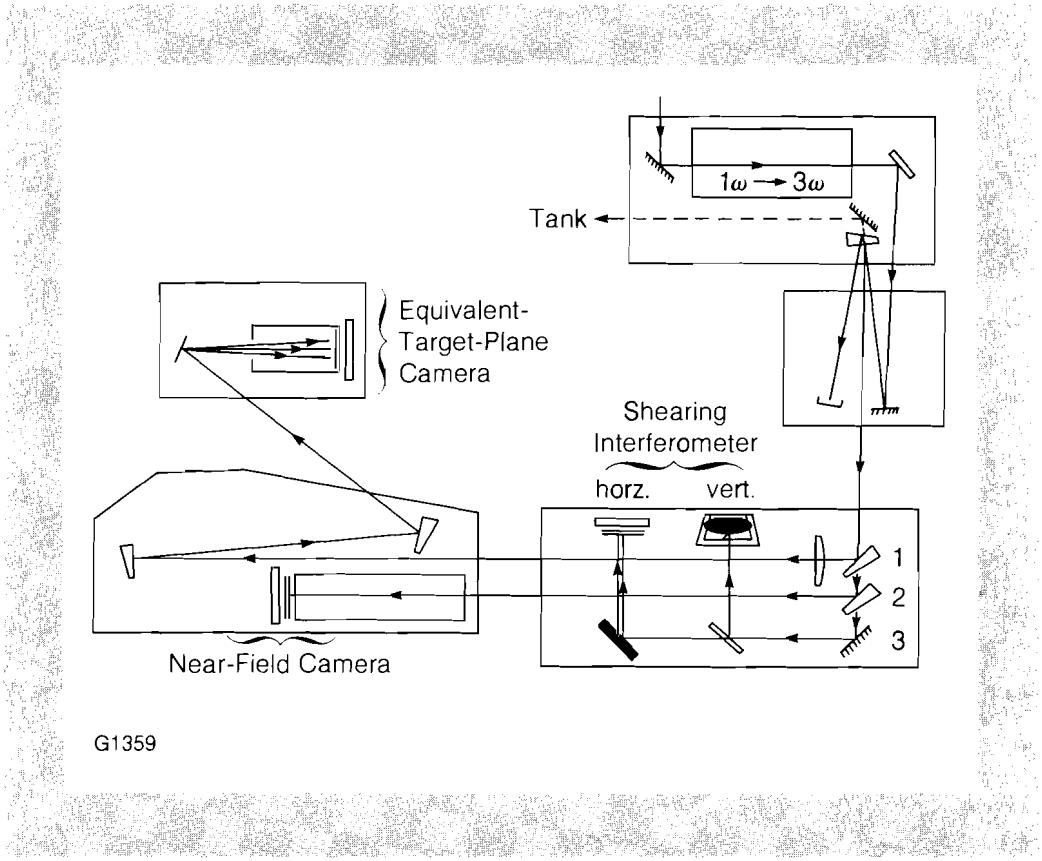

Fig. 18.3
The conventional experimental setup includes a near-field (NF) camera, an equivalent-target-plane (ETP) camera, and a lateral-shearing interferometer with two orthogonally oriented shear plates.

range in the recording medium. The second path directed the beam into a near-field camera, while the third path was used for lateral-shearing interferometry. The two slightly wedged plates, orthogonally oriented, shear the laser beam to produce fringes that represent loci of constant wave-front slope.

These wave-front-measurement techniques provided a good characterization of the GDL frequency-converted laser beam. Figure 18.4 shows the photographic result of a 1-D ETP array, a near-field photograph, and horizontal and vertical lateral-shearing interferograms. Defects in the conversion crystals were located, and distortions in the crystal cell were found. The equivalent target plane, representing tangential focus, was accurately recorded without image distortion. A quantitative analysis of the interferogram was not performed, since a visual inspection clearly indicated a severe aberration problem in the beam. A subsequent interferometric study of the frequency-conversion crystals and crystal cells determined that they were the source of most of the phase error. However, the lateral-shearing interferometry does not record the phase front of the beam in a form which is easy to interpret. The equivalent-target-plane camera has not been proved to be successful at the exact focus of the lens. A holographic technique is capable of producing both a 2-D map of the phase front, and a continuum of ETP images that approach the focal plane, thus offering interferometric and intensity-measurement capabilities not presently available for pulsed-beam analysis.

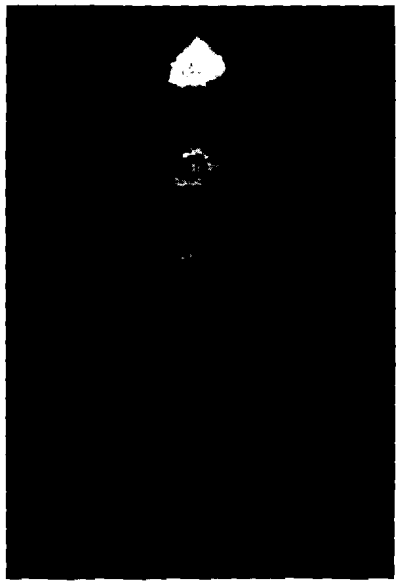

Equivalent-Target-Plane
Array (true size)

0 (mm) 125
Near Field

Vertical Shear

Horizontal Shear

G1338

Fig. 18.4
The photographic results of the conventional wave-front-measurement techniques include a 1-D ETP array in exposure, a near-field image, and two orthogonally oriented shearing interference patterns.

Holographic Wave-Front Recording and Reconstruction

Holography is a method of recording and reconstructing the complex amplitude of a wave front. This is achieved by recording the interference pattern between an object wave front and a coherent reference beam. The use of a silver halide emulsion as an energy-recording medium requires chemical processing in order to manifest the wave-front modulation. Wave-front reconstruction takes place, in a third step, when the hologram is illuminated with a second reference wave. Under certain conditions, the reconstructed wave front is identical in form to the original wave front, and may be manipulated as if it were the original beam.

Expressions describing the interference and modulation between the object wave and the reference wave show the means by which the amplitude and relative phase information are preserved. Let the object wave and reference wave be represented, respectively, by

$$\text{(Object)} \quad O(x,y)e^{i[-\omega_1 t + \alpha x + \gamma z + \psi(x,y)]}$$

$$\text{(Reference)} \quad R(x,y)e^{i[-\omega_2 t + \delta x + \mu z + \phi(x,y)]}$$

where $O(x,y)$, $\psi(x,y)$ and $R(x,y)$, $\phi(x,y)$ represent the amplitude and phase distribution pairs of the object and reference waves, respectively (see Fig. 18.5). The relationships between the incident angles, χ and θ, and the pairs of propagation constants, α, γ, and δ, μ of the object wave and reference wave, respectively, are the following:

$$\alpha = k \sin \chi, \; \gamma = k \cos \chi$$

$$\delta = k \sin \theta, \; \mu = k \cos \theta.$$

The temporal frequencies, ω_1 and ω_2, have units of radians/second. Square law detection of the interference signal between these two waves by the holographic plate produces a signal, $S(x,y)$, described by

$$S(x,y) \propto O^2(x,y) + O(x,y)R(x,y)\, e^{i[2\alpha x + \psi(x,y) - \phi(x,y)]} + R^2(x,y) + O(x,y)R(x,y)\, e^{-i[2\alpha x + \psi(x,y) - \phi(x,y)]}. \quad (1)$$

Wave-front reconstruction is achieved by propagating a second reference wave through the holographic plate. Let the new reference wave be represented by $W(x,y)$,

$$W(x,y) = R'(x,y)e^{i[-\omega t + \epsilon x + \Omega(x,y)]}$$

where ϵ is the propagation constant, $\epsilon = k \sin \beta$, and β is the incident angle of the reference beam. $R'(x,y)$ and $\Omega(x,y)$ represent the amplitude and phase distribution of the new reference beam. If the reconstructing wave propagates along the same path as the original reference wave then the object amplitude is given by

$$E_{obj} = R'(x,y)O(x,y)R(x,y)\, e^{i[-\omega t + \alpha x + \Psi(x,y) - \phi(x,y) + \Omega(x,y)]}. \quad (2)$$

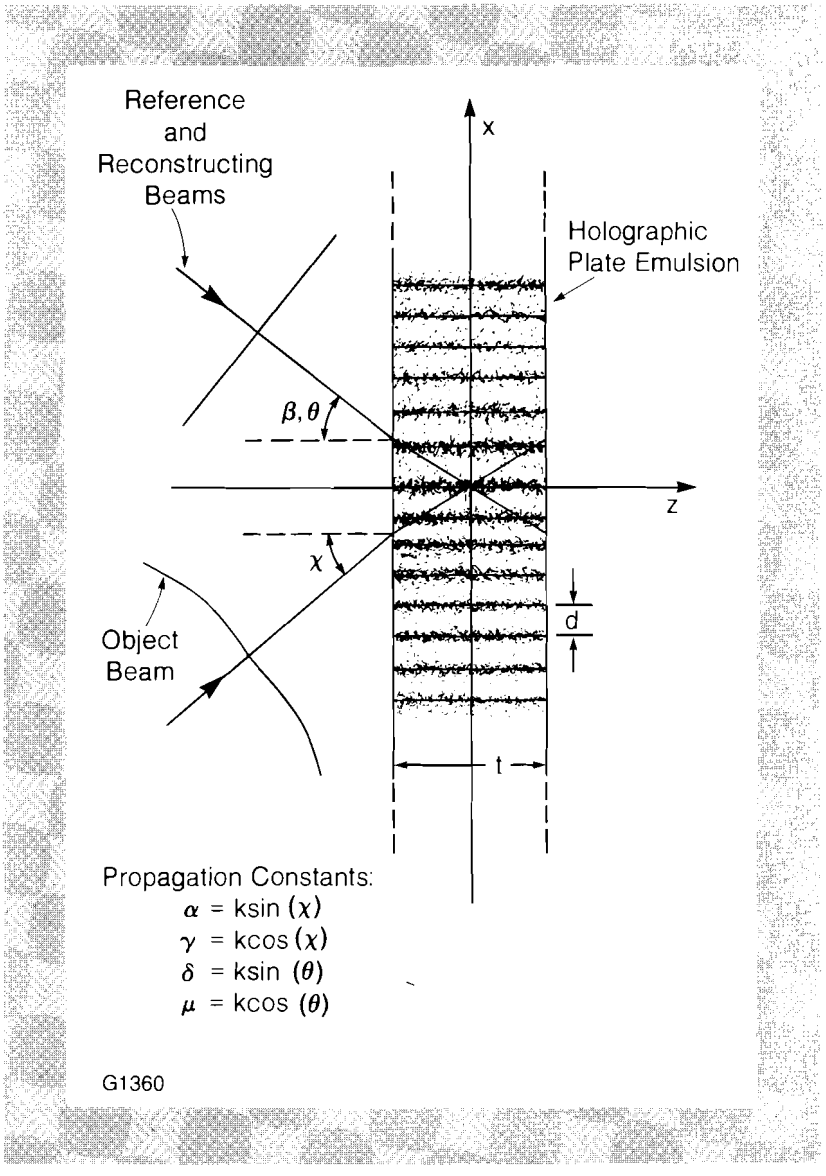

Fig. 18.5
The object and reference beams interfere symmetrically with respect to the normal to the holographic plate so that $\theta = -\chi$. The cw reconstructing-reference beam follows the same path as the pulsed-reference beam so that $\beta = \theta$.

The propagation constant, α = ksin χ, shows that the reconstructed object wave travels along the same path as the original object wave. Equation (2) shows that nominally plane-wave reference beams, containing slowly varying phase errors, are adequate as reference beams as long as the condition that $\Omega(x,y) - \phi(x,y)$ = constant is satisfied. Differences between the two phase distributions translate directly into the phase distribution of the reconstructed object wave. Equation (2) also shows that any amplitude nonuniformities, in either reference wave, translate directly into nonuniformities in the reconstructed-object amplitude. Therefore, linear recording of the object beam requires that the holographic system be able to select a portion of the original wave, and produce from it a uniform amplitude distribution to serve as the reference beam.

The filtering of the high-frequency Fourier components of a wave front results in increased amplitude uniformity. A system which is

capable of making the spatial-frequency spectrum physically accessible, for accurate filtering, is shown in Fig. 18.6. An entrance lens is placed at the center of a large obstruction, and used to expand a small portion of the original wave. The recollimation of this beam produces a plane-wave reference, which is a relatively simple phase distribution to reproduce. For a wave front with several wavelengths of aberration, a small portion of the wave front possesses a small fraction of a wavelength in phase variation, guaranteeing a nominally plane reference wave.

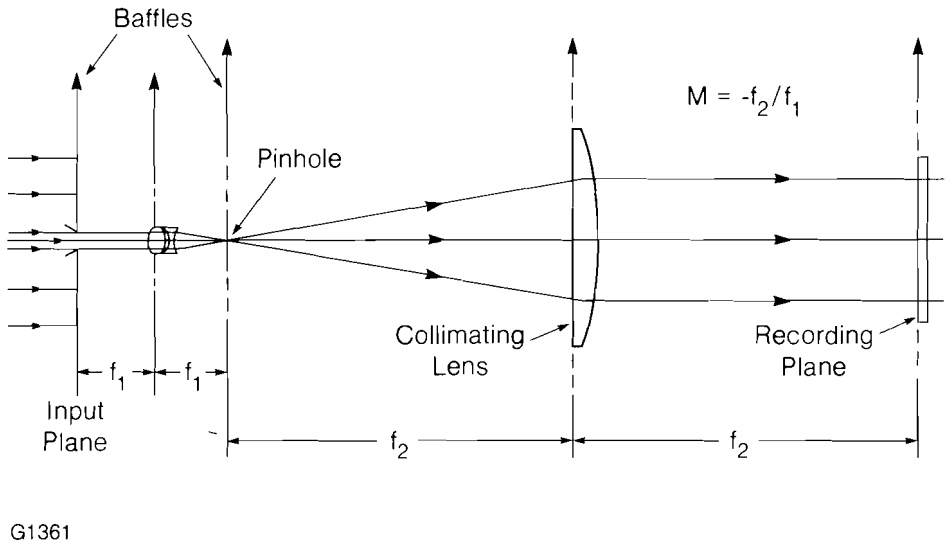

Fig. 18.6
The spatial filter system selects a 3.8-mm-diameter portion of the pulsed beam, filters out the high frequency content with a 15-μm pinhole, and produces a more uniform plane-wave reference beam at the holographic recording plane ($M = -f_2/f_1 = 22$).

The heart of the holographic experimental setup (Fig. 18.7) is a holographic interferometer. The use of a Galilean down-collimating telescope allowed a compromise between studying the GDL-pulsed wave front and using standard-format, 5″ by 4″, Agfa-Gevaert 10E56 holographic plates. The incident wave front was split into a reflected-object beam and a transmitted-reference beam. A central region of the transmitted beam continued through an input aperture, passed through focus to be filtered, and was recollimated. A magnification of ~ 22 produced an 83-mm-diameter reference beam which overfilled the 63-mm-diameter demagnified object beam. The two beams recombined at the holographic plate to form an interference pattern that was characteristic of both the object and the reference beam. A cw laser, operating at the same wavelength, was used with the same setup to reconstruct the object wave front.

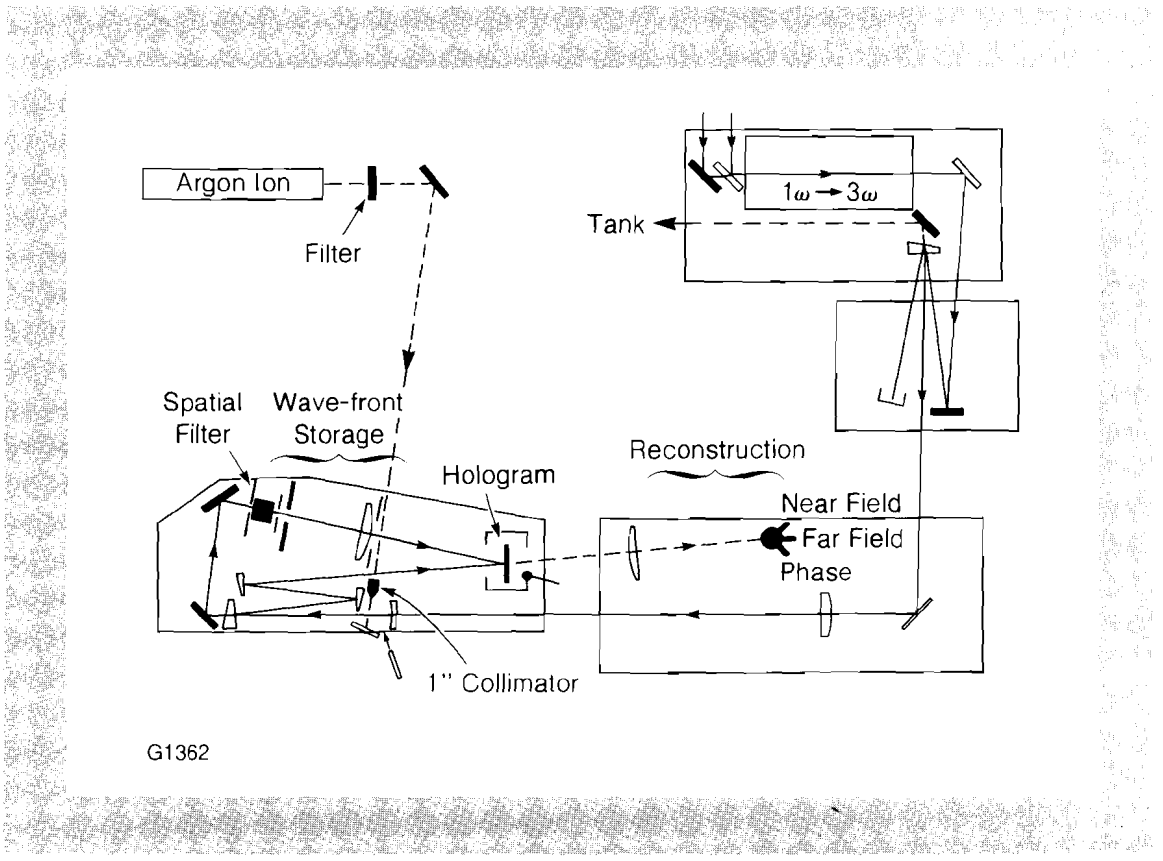

Fig. 18.7
The holographic experimental setup consists of two systems. First, the wave-front storage system includes beam-steering optics which direct the pulsed beam through the two arms of the holographic interferometer, where the reference beam path is delineated by the spatial filter and the object beam path contains three bare surface reflectors. The two paths cross at the holographic recording plane, where the interference pattern between the pulsed object and reference beam is stored in the form of a hologram. Secondly, the wave-front reconstruction system includes a cw argon ion laser which is injected into the reference beam path to produce a colinear reconstructing plane-wave reference beam. The reconstructed wave front that emanates from the hologram is measured by means of near-field and far-field cameras and several interferometers.

Holographically Reconstructed Wave-Front Measurement

Conventional wave-front-measurement techniques were applied to both the reconstructed beam and the pulsed beam in order to provide a means of evaluation for the holographic technique. The image-processing system at the LLE was used to digitize and intensity-correct the photographic data, and to perform computer-based manipulations and statistical calculations on these images. Reconstructed near-field (Figs. 18.8 and 18.9) and quasi-far-field (Figs. 18.10 and 18.11) intensity distributions closely resemble those obtained from conventional techniques. Reconstruction of the near-field intensity profile was achieved with an overall resolution approaching 2 lines/mm, and an azimuthally averaged, peak-to-valley intensity-modulation increase of about 50%. The resolution of the reconstructed quasi-far-field intensity profile was nearly the same, 1-2 lines/mm, but the peak-to-valley intensity-modulation increase was 90%. The resolution was limited by both halation effects and scattering at the holographic plate. The intensity-modulation increase is symptomatic of a nonlinearly recorded amplitude distribution, attributable to an excessive object-to-reference beam-intensity ratio and amplitude nonuniformities in the pulsed-reference beam.

Figure 18.12 shows both the pulsed and the reconstructed-object-beam lateral-shearing interferograms. A direct comparison can be made since the amount of shear is, within a few percent, the same. The time-dependent phase effects, clearly evident in the pulsed interferogram, are reduced in the reconstructed interferogram. The

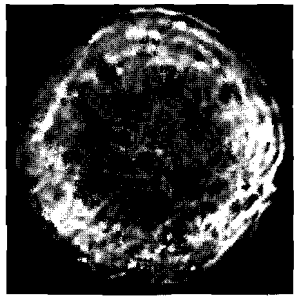

(a) Original Print

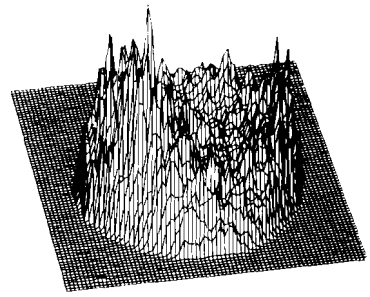

(b) 3-D Intensity Plot

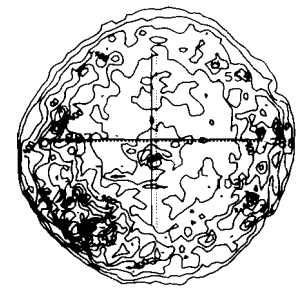

(c) Iso-Intensity Contour Plot

G1340

Fig. 18.8
A near-field photograph of the demagnified GDL frequency-tripled laser beam is used as a point of reference for evaluation of the holographically produced near-field distribution.

(a) Original Print

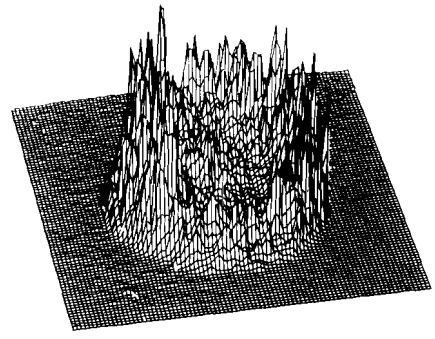

(b) 3-D Intensity Plot

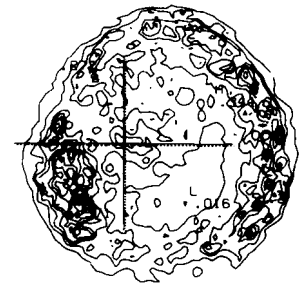

(c) Iso-Intensity Contour Plot

G1339

Fig. 18.9
The reconstructed near-field intensity distribution closely resembles the pulsed near-field profile, but a modulation increase due to non-linear recording is evident.

number of fringes, as well as their orientation, is the same in each pattern. Small, rapidly varying changes in the shape of each fringe, of the same magnitude observed between measurements of different laser pulses, are present. Additionally, small, slowly varying differences in the shape of the fringes corresponding to optical-path differences of about one-half to one wavelength of light, are readily attributable to OPD variations in the holographic plate.

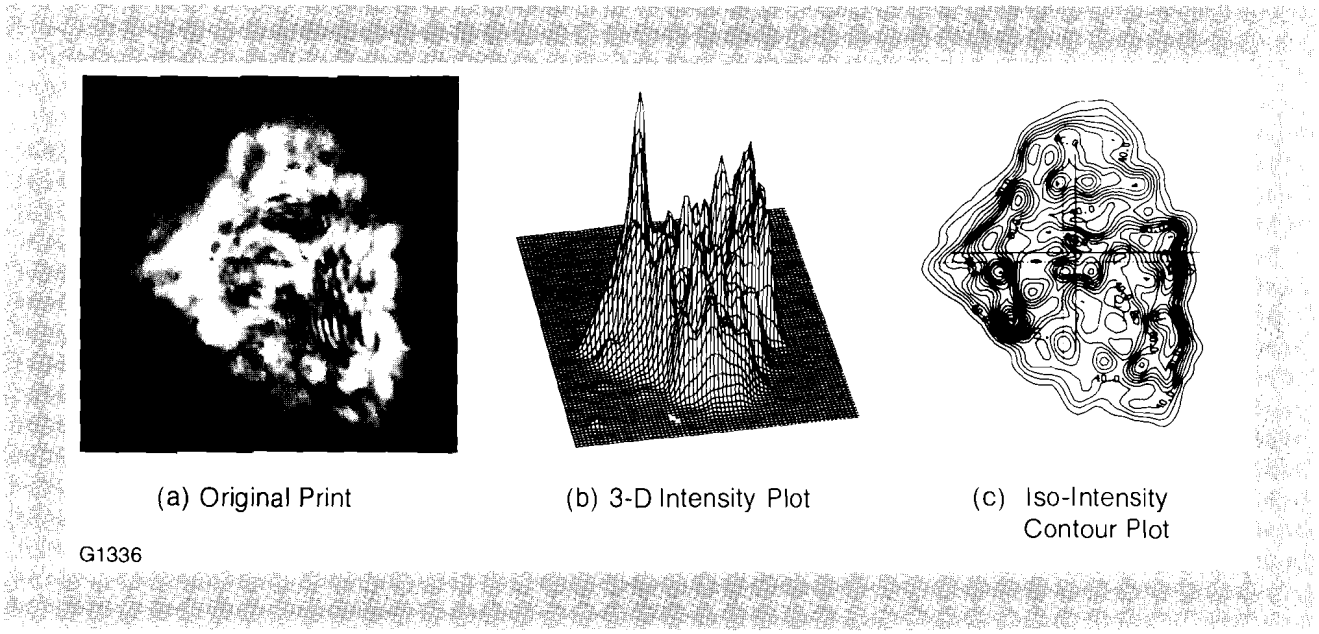

Fig. 18.10
A far-field photograph of the GDL frequency-tripled laser beam is used as a point of reference for evaluation of the holographically produced far-field distribution.

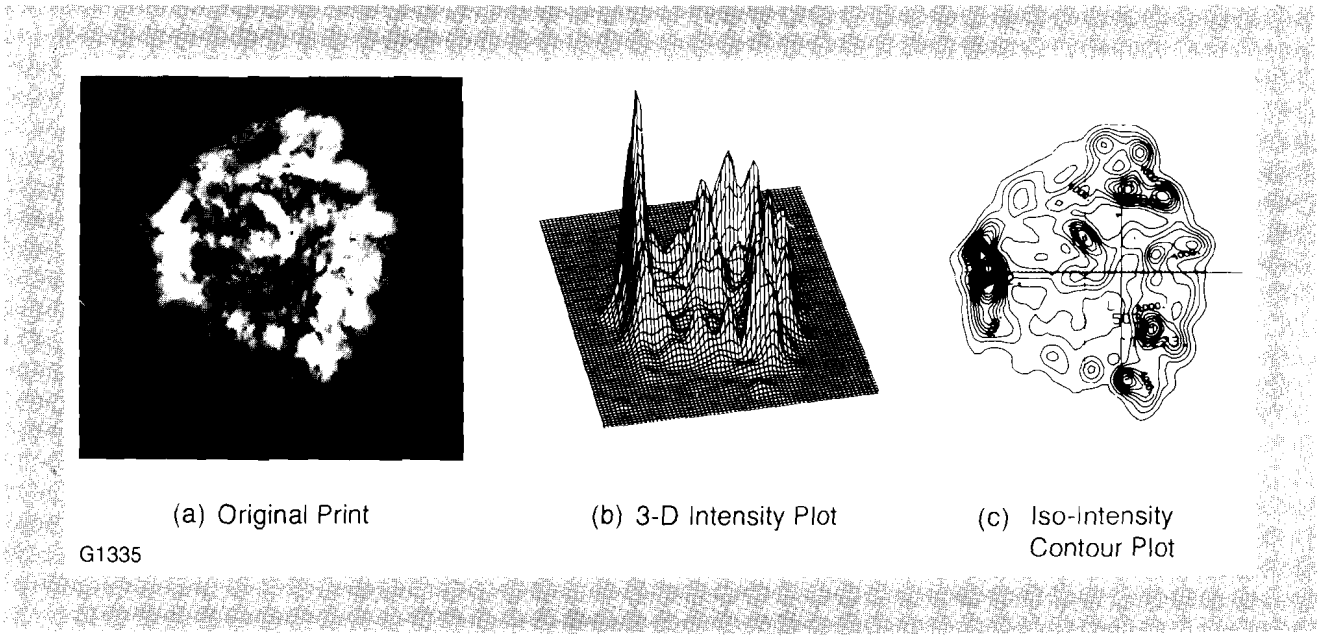

Fig. 18.11
The reconstructed ETP array closely resembles the pulsed ETP results, but nonlinear recording and OPD errors presently limit the accuracy of far-field imaging.

The final experiment at $\lambda = 351$ nm, conducted on the reconstructed object wave front, produced a 2-D measurement of the phase front. A bleached hologram was placed at the original recording plane. A point-diffraction interferometer (Smartt PDI) was positioned at the focus of an F/3 lens, and a UV vidicon camera was placed

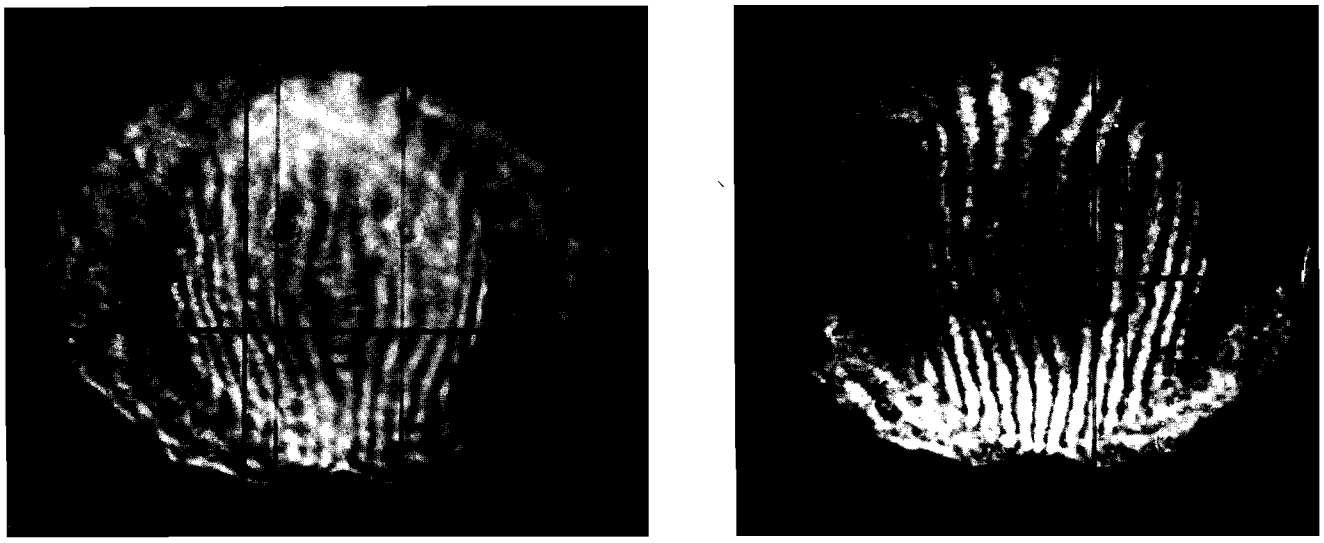

pulsed reconstructed

G1337

Fig. 18.12
Lateral-shearing interferograms provide information about the derivative of the phase front. Pulsed and reconstructed interferograms have the same number of fringes and the same orientation, indicating an accurate phase-front reconstruction.

immediately behind the PDI to aid in the alignment of the interferometer. An interferogram obtained with the point-diffraction interferometer is shown in Fig. 18.13(a). It represents the cumulative phase distortion due to the object beam, the holographic plate, the focusing lens, and the defocus introduced by the axial position of the PDI pinhole. Large variations in the fringe visibility, inherent in the application of the PDI to highly aberrated phase fronts, are observed. An additional experiment was performed to determine the requirements for conventional holographic interferometry. A holographic interferometer was constructed on a pneumatically stabilized optical table. The reconstructing and reference beams were derived from a Helium-Neon laser. The reconstructed wave front was combined with the directly transmitting wave front from the other arm of the system to form two-beam interference fringes as shown in Fig. 18.13(b). The OPD variations of the holographic plate were removed from the interference pattern by passing the reference beam through the plate, coincident with the reconstructed beam. Eight to nine defocus fringes are counted from center to edge. These correspond to 8.5 wavelengths of defocus at $\lambda = 632.8$ nm, or about 15 wavelengths at $\lambda = 351.1$ nm. The seven to eight fringes over half of the field of the shearing interferograms also correspond to $\sim$ 15 wavelengths of defocus at $\lambda = 351.1$ nm. With defocus as the measure of comparison, the shearing interferometry is in close agreement with the holographic interferometry.

Summary

Holographic techniques have been successfully implemented on a UV, frequency-tripled, high-peak-power laser in order to obtain cw reconstructions for conventional wave-front measurements. Near-field amplitude and phase distributions from the GDL frequency-converted laser have been holographically recorded on silver-halide emulsions. Previously the absence of a suitable reference beam forced one to use some type of shearing interferometry to obtain phase-front information, while the near-field and far-field distributions

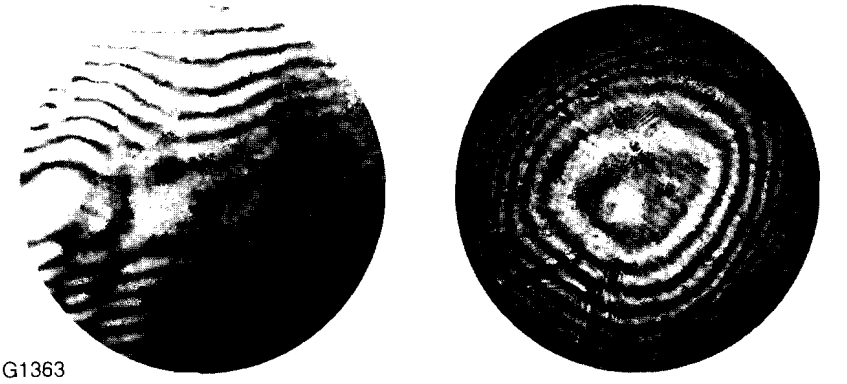

(a) Point-Diffraction Interferometer

(b) Holographic Interferometer

Fig. 18.13
The point-diffraction interferometer (a) yields 2-D phase-front information by means of a locally generated reference beam derived from the aberrated point-spread function of the test wave front. The holographic interferometer (b) yields 2-D phase-front information by means of a separate plane-wave reference beam. The difference between these results is primarily a defocus term in the point-diffraction interferogram (a).

were recorded as intensity profiles. A spatially filtered, locally generated reference beam was created to holographically store the complex amplitude distribution of the pulsed laser beam, while reconstruction of the original wave front was achieved with a cw laser.

Although the reconstructed intensity profiles closely resemble those obtained from conventional methods, we conclude that this technique does not presently reproduce the laser amplitude distribution with sufficient accuracy to replace conventional intensity measurement techniques. However, it is believed that several improvements can be made, especially with regard to system flexibility, that would greatly reduce the sources of noise and the sources of nonlinear amplitude recording. Furthermore, this technique presently provides the means to study the relationship between phase correction (wave-front modulation) and the corresponding changes in the intensity distribution at the real target plane.

Accurate phase-front reconstruction was demonstrated, with the optical path variations of the holographic plate limiting the measurement accuracy to one-half wave ($\lambda = 351$ nm) for the central 75% of the beam's area, and to one wave for the edge of the beam. Additionally, several two-beam interferometric techniques, not practicable with a high-peak-power laser, have been successfully implemented on a cw reconstruction of the pulsed laser beam.

ACKNOWLEDGMENT

This work was supported by the U.S. Department of Energy Office of Inertial Fusion under contract number DE-AC08-80DP40124 and by the Laser Fusion Feasibility Project at the Laboratory for Laser Energetics which has the following sponsors: Empire State Electric Energy Research Corporation, General Electric Company, New York State Energy Research and Development Authority, Northeast Utilities Service Company, Southern California Edison Company, The Standard Oil Company, and University of Rochester. Such support does not imply endorsement of the content by any of the above parties.

REFERENCES

1. LLE Review **12**, 5 (1982).

2. LLE Review **7**, 5 (1981).